HEFAT2007
5th International Conference on Heat Transfer, Fluid Mechanics and Thermodynamics
Sun City, South Africa
Paper number: JS2

A NUMERICAL STUDY OF HEAT AND MASS TRANSFER IN AN ADSORPTION TYPE HYDROGEN STORAGE TANK

Jensen S.*, Næss E., Bünger U. and Sønju O.
*Author for correspondence
Department of Energy and Process Engineering,
Norwegian University of Science and Technology (NTNU),
Kolbjørn Hejes vei 1b,
7491 Trondheim,
Norway,
E-mail: stian.jensen@ntnu.no

ABSTRACT

In this paper numerical solutions of a mathematical model that describes the heat transfer, the fluid flow and the sorption process in a cylindrical adsorption type hydrogen storage tank are presented. The tank operates at cryogenic temperatures and the storage approach is intended for use in automotive applications. The model is solved using the spectral element method combined with an overall third order accurate time stepping scheme. Numerical experiments show that the time to fill the tank decreases with increasing charging pressure and that low conductive heat fluxes constrain the filling process.

INTRODUCTION

Hydrogen is one possible candidate as a future fuel in automobiles. However, due to its low density it is not easily stored on-board vehicles. The main challenges are to reduce the volume and the weight of the storage vessel to hold the required amount of hydrogen for sufficient mileage. One possibility is to fill the storage vessel with a fine grained adsorbent that possesses a high specific surface area (SSA) such that hydrogen can be adsorbed on the surface of the adsorbent particles. When adsorbed, hydrogen is bonded to the surface by van der Waals forces that are greater in magnitude than the intermolecular forces. In that manner the molecules are potentially packed closer together than in the pure gaseous phase.

Another storage strategy is to chemi-sorb hydrogen in metal hydrides. This approach has received extensive attention in the literature with respect to modeling of heat and mass transfer, see e.g Refs. [1–3] and the references therein. Although some metal hydrides can be operated at ambient temperature and moderate pressures, they still suffer from low gravimetric storage densities. This has triggered interest in adsorption type storage systems. The heat and mass transfer of these systems, on the other hand, have not been studied as intensively [4, 5] and very little attention has been devoted to the transient thermal analysis of cryogenic storage systems in particular. Such an analysis is attractive since the adsorption capacity is increased when lowering the temperature.

Hydrogen sorption is an exo-/endothermal reversible process, such that during filling the tank needs to be cooled, and upon discharge the tank needs heat input. During discharge, hydrogen is dispatched at a relatively low mass flow rate whereas during filling the mass flow rates are much higher. Accordingly, the absolute values of the heat transfer rates are much higher during filling than during discharge. This fact renders the filling process the challenging step from an operational point of view, and for that reason it is the focus of the present paper. In this work a particular and readily available activated carbon, namely NORIT R0.8 EXTRA, is applied as the adsorbent in agreement with an ongoing experimental research program at the department. In fact, the objectives of this study is to predict the transient behavior of the experimental storage tank, which is submerged in a dewar with liquid nitrogen, alongside establishing a general numerical test bed.

MATHEMATICAL MODEL

The porous matrix of the activated carbon together with the hydrogen gas make up a porous medium as visualized in Fig. 1. Here, β denotes the fluid phase, i.e. the hy-

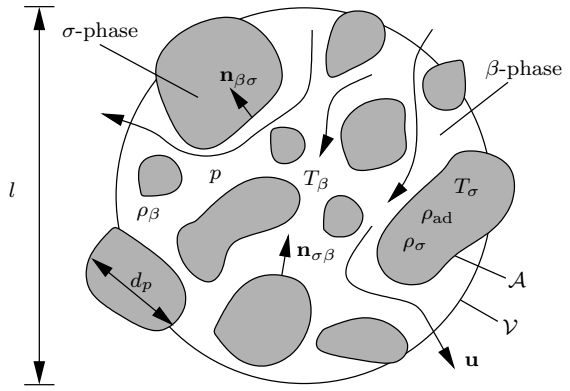

Figure 1: The two-phase porous medium composed of the β-phase and the σ-phase. Symbols are described in the text.

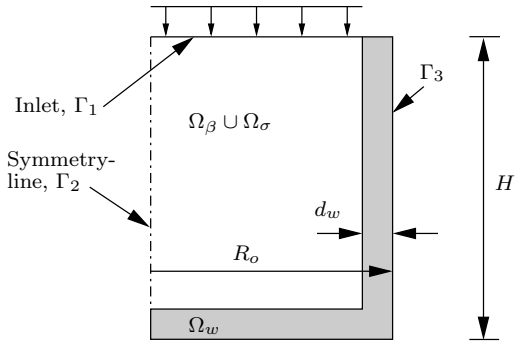

Figure 2: Schematic view of the storage vessel and, hence, the computational domain $\Omega = \Omega_\beta \cup \Omega_\sigma \cup \Omega_w$. The shaded area represents the tank walls, $\Gamma = \Gamma_1 \cup \Gamma_2 \cup \Gamma_3$ is the boundary of Ω, R_o is the outer radius, d_w is the wall thickness and H is the height.

drogen gas, and σ denotes the solid phase including both the carbon particles and the adsorbed hydrogen. Furthermore, d_p denotes a typical particle diameter, l is the microscopic length scale, $\mathbf{u}$ is the hydrogen velocity vector field, p is the hydrogen pressure, T_β and T_σ are the temperature fields of, respectively, the β- and σ-phases, ρ_{ad} is the density of adsorbed hydrogen, ρ_β is the density of the hydrogen gas, and $\mathbf{n}_{\beta\sigma} = -\mathbf{n}_{\sigma\beta}$ are unit normal vectors.

Governing equations. In this work, the hydrogen flow is assumed to be semi-incompressible which implies that the transient term in the gas phase continuity equation is dropped $\partial_t \rho_\beta = 0$. The hydrogen gas phase density is described by the ideal gas law, which is justified by the fact that the compressibility factor is close to unity for the pressure and temperature ranges analyzed. Furthermore, the transport properties, i.e. hydrogen viscosity μ, thermal conductivities of the the two phases λ_β and λ_σ and effective hydrogen self-diffusivity $\mathscr{D}_{\text{eff}}$ in the particles, are treated as constants. Also, gravity forces, compression work and thermal radiation effects are neglected. Hence, at the microscopic scale the governing equations for momentum-, mass- and energy conservation for the two phases can be posed as

$$\partial_t \rho_{\text{ad}} = \mathscr{D}_{\text{eff}} \nabla^2 \rho_{\text{ad}} \quad \text{in} \quad \Omega_\sigma \tag{1}$$

$$\rho_\beta(\partial_t \mathbf{u} + \mathbf{u} \cdot \nabla \mathbf{u}) = -\nabla p + \mu \nabla^2 \mathbf{u} \quad \text{in} \quad \Omega_\beta \tag{2}$$

$$\nabla \cdot \rho_\beta \mathbf{u} = 0 \quad \text{in} \quad \Omega_\beta \tag{3}$$

$$(\rho c_p)_\beta(\partial_t T_\beta + \mathbf{u} \cdot \nabla T_\beta) = \lambda_\beta \nabla^2 T_\beta \quad \text{in} \quad \Omega_\beta \tag{4}$$

$$(\rho c_p)_\sigma \partial_t T_\sigma = \lambda_\sigma \nabla^2 T_\sigma \quad \text{in} \quad \Omega_\sigma \tag{5}$$

with appropriate boundary conditions. Here, the domains Ω_β and Ω_σ describe the regions in space occupied by the two phases, and the complete tank domain is described by $\Omega = \Omega_\beta \cup \Omega_\sigma \cup \Omega_w \in \mathbb{R}^d$, where Ω_w is the region of the tank walls, as shown in Fig. 2. The subscript β has deliberately been dropped for brevity for p, $\mathbf{u}$ and μ, since these are unique to the β-phase, i.e. they are only defined in Ω_β. Similarly, the subscript σ is dropped for ρ_{ad}. When posing (1) it has already been assumed that the equation has been spatially smoothed within the particles, such that $\mathscr{D}_{\text{eff}}$ is the effective self-diffusivity of hydrogen in the micro-pores of the particles.

Local volume averaging and closing. Although, the set of equations (2)-(5) are valid at the microscopic level, under the aforementioned assumptions, they are not easily solved in their respective domains since Ω comprises millions of particles. Hence, some kind of up-scaling is necessary. To this end the method of local volume averaging [6] can be applied. The local volume average (LVA) of, say, the temperature of the β-phase is defined as

$$\langle T_\beta \rangle = \varepsilon \langle T_\beta \rangle^\beta = \frac{1}{\mathcal{V}} \int_{\mathcal{V}_\beta} T_\beta \, dV \tag{6}$$

where $\mathcal{V} = \mathcal{V}_\sigma \cup \mathcal{V}_\beta \in \Omega$ is a small representative region in space as shown in Fig. 1, $\mathcal{V}_\beta$ is the volume occupied by the β-phase and the porosity is defined as $\varepsilon = \mathcal{V}_\beta / \mathcal{V}$. Here, $\langle T_\beta \rangle$ denotes the superficial average and $\langle T_\beta \rangle^\beta$ denotes the intrinsic average of T_β. Together with (6), two LVA theorems are needed to smooth the equations, these are

$$\langle \nabla T_\beta \rangle = \nabla \langle T_\beta \rangle + \frac{1}{\mathcal{V}} \int_{\mathcal{A}} T_\beta \mathbf{n}_{\beta\sigma} \, dA \tag{7}$$

$$\langle \nabla \cdot \mathbf{q}_\beta \rangle = \nabla \cdot \langle \mathbf{q}_\beta \rangle + \frac{1}{\mathcal{V}} \int_{\mathcal{A}} \mathbf{q}_\beta \cdot \mathbf{n}_{\beta\sigma} \, dA \tag{8}$$

where $\mathcal{A}$ is the interfacial surface area contained in $\mathcal{V}$. After the application of (6)-(8), closure constitutive equations are needed to close the equations. In this work we typically employ empirical constitutive equations found in the literature or heuristic relationships where appropriate.

To arrive at the equations presented below, some more assumptions need to be made. The two phases are considered to be in local thermal equilibrium (LTE), i.e. $\langle T \rangle = \langle T_\beta \rangle^\beta = \langle T_\sigma \rangle^\sigma$. Additionally, the particles are treated as perfect spheres with diameter d_p, the porosity ε is constant and the porous medium is isotropic with respect to transport processes.

Adsorption. The linear driving force (LDF) model [7] simplifies (1) to an ordinary differential equation (ODE)

$$\langle \dot{\rho}_{\text{ad}} \rangle = k_L(\langle \rho^*_{\text{ad}} \rangle - \langle \rho_{\text{ad}} \rangle) \quad \text{in} \quad \Omega \tag{9}$$

valid at the macroscopic level. Here, k_L is the effective LDF mass transfer coefficient (cf. Hills [8])

$$k_L = 60\mathscr{D}_{\text{eff}}/d_p^2$$

and $\langle\rho^*_{\text{ad}}\rangle$ is the LVA density of adsorbed hydrogen under equilibrium conditions given by an adsorption equilibrium isotherm as discussed below. The total density of stored hydrogen $\langle\rho_{\text{tot}}\rangle$ in the tank can then be expressed as

$$\langle\rho_{\text{tot}}\rangle = (1/\varepsilon)\langle\rho_\beta\rangle + \langle\rho_{\text{ad}}\rangle = \langle\rho_\beta\rangle^\beta + \langle\rho_{\text{ad}}\rangle \qquad (10)$$

i.e. the sum of hydrogen that would be contained in an adsorbent free vessel and excess adsorbed hydrogen. The effective self-diffusivity is then given by [9]

$$\mathscr{D}_{\text{eff}} = [2\varepsilon_\mu/(3-\varepsilon_\mu)]\mathscr{D}$$

where ε_μ is the micro-porosity of the particles. The self-diffusivity of hydrogen $\mathscr{D}$ is determined from kinetic theory of gases at fixed and typical temperature and pressure values (see Tab. 1).

NORIT R0.8 is, to the best of the present authors knowledge, not fully characterized in the open literature with respect to adsorption equilibrium isotherms. Hence, we propose a way of establishing such an isotherm by capitalizing on the following. It has been observed through experiments that there is a nearly linear dependence between hydrogen adsorption capacity and SSA amongst activated carbons [10]. Bénard and Chahine [11] characterized another activated carbon, AX-21, thoroughly and investigated different models, one of which is a Langmuir model

$$\langle\rho^*_{\text{ad}}\rangle = \mathcal{K}\langle p\rangle^\beta/(1+\mathcal{K}\langle p\rangle^\beta)\langle\rho_{\text{sat}}\rangle \qquad (11)$$

This model can be adapted to NORIT R0.8 by correcting the saturation density $\langle\rho_{\text{sat}}\rangle$ given in Ref. [11] by the ratio of the SSAs of the two adsorbents such that

$$\langle\rho_{\text{sat}}\rangle = 100/(1+0.035\langle T\rangle)M_{\text{H}_2}(\text{SSA}_{\text{NOR}}/\text{SSA}_{\text{AX}})\langle\rho_\sigma\rangle$$

where M_{H_2} is the molecular weight of hydrogen. The equilibrium constant $\mathcal{K}$ follows an Arrhenius expression

$$\mathcal{K} = A\exp[E_A/(R\langle T\rangle)]$$

All parameters related to the isotherm are given in Tab. 1. The adapted excess adsorption equilibrium isotherm for NORIT R0.8 is shown in Fig. 3 where it is compared to the data-points of Texier-Mandoki *et al.* [12]. Also shown in the figure is an Ono-Kondo isotherm where 5 adsorption layers have been assumed. This isotherm was adapted from Refs. [11, 13] by correcting the relevant properties with the differences in SSAs, in a similar fashion as above. The Ono-Kondo model is assumably more accurate over wider pressure and temperature regimes than (11). However, this model requires the solution of non-linear equations for the concentration of the adsorbate in each layer, so, due to its simplicity, the Langmuir model is adopted in this work.

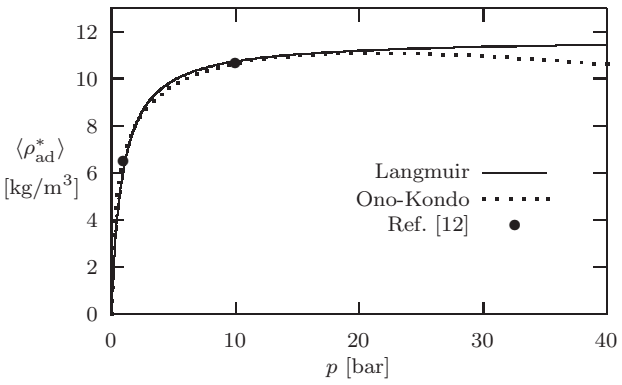

Figure 3: The adapted excess adsorption equilibrium isotherms at $T = 77$ K for NORIT R0.8 are compared to the data-points of Texier-Mandoki *et al.* [12].

It can be noted that this adsorbent would require a tank volume of 160 dm^3 to hold a typical amount of 4 kg of hydrogen at $p = 40$ bar without considering insulation and the pressure vessel itself. Hence, this is not a suitable adsorbent for practical applications. It is sufficient for research purposes, however, since the point of interest lies in assessing the qualitative behavior.

Momentum equations. Darcy's law is valid for vanishing Reynolds numbers based on the particle diameter and the so-called Darcian velocity $\langle\mathbf{u}\rangle$, i.e. $Re_{d_p} = \langle\rho_\beta\rangle^\beta|\langle\mathbf{u}\rangle|d_p/\mu < 1$. With the assumption of an isotropic porous medium the permeability tensor is reduced to a scalar K and we obtain the following smoothed momentum equations

$$0 = -\nabla\langle p\rangle^\beta - \mu/K\langle\mathbf{u}\rangle - \langle\dot\rho_{\text{ad}}\rangle\langle\mathbf{u}\rangle \quad \text{in } \Omega \qquad (12)$$

The last term on the right hand side compensates for the loss of momentum due to interphasial mass transfer. The latter term stems from the application of (8) to the convection term in (2) using the following heuristic closure

$$\langle\dot\rho_{\text{ad}}\rangle\langle\mathbf{u}\rangle = \frac{1}{\mathcal{V}}\int_{\mathcal{A}}\rho_\beta\mathbf{u}\mathbf{u}\cdot\mathbf{n}_{\beta\sigma}\,dA$$

The permeability K is given by (see e.g. Ref. [14])

$$K = (d_p^2\varepsilon^3)/[180(1-\varepsilon)^2]$$

Continuity equation for the hydrogen gas. The local volume averaged continuity equation is

$$\nabla\cdot\langle\rho_\beta\rangle^\beta\langle\mathbf{u}_\beta\rangle = -\langle\dot\rho_{\text{ad}}\rangle \quad \text{in} \quad \Omega \qquad (13)$$

where it is assumed that the density of the hydrogen gas ρ_β is constant over the small averaging volume $\mathcal{V}$. The case $\langle\dot\rho_{\text{ad}}\rangle > 0$ corresponds to adsorption and the case $\langle\dot\rho_{\text{ad}}\rangle < 0$ corresponds to desorption. The right hand side

is obtained by using

$$\langle \dot{\rho}_{\text{ad}} \rangle = \frac{1}{\mathcal{V}} \int_{\mathcal{A}} \rho_\beta \mathbf{u} \cdot \mathbf{n}_{\beta\sigma} \, dA$$

after the application of (8) to (3).

Energy equation. By the aforementioned LTE assumption a single energy equation is constructed for the porous medium

$$\left.\begin{aligned} (\rho c_p)_{\text{eff}} \partial_t \langle T \rangle + \langle \rho_\beta \rangle^\beta c_{p,\beta} \langle \mathbf{u} \rangle \cdot \nabla \langle T \rangle = \\ \nabla \cdot \mathbf{\Lambda}_{\text{eff}} \cdot \nabla \langle T \rangle - \Delta H \langle \dot{\rho}_{\text{ad}} \rangle \end{aligned} \right\} \text{ in } \Omega \qquad (14)$$

where $-\Delta H$ is the heat of adsorption and the effective heat capacity is given by

$$(\rho c_p)_{\text{eff}} = \langle \rho_{\text{tot}} \rangle c_{p,\beta} + \langle \rho_\sigma \rangle c_{p,\sigma}$$

The last term on the right hand side of (14) accounts for the heat released during adsorption. In the derivation of this equation we have benefited from (7) and (8) in addition to the spatial decomposition formula

$$T_\beta = \langle T_\beta \rangle^\beta + T'_\beta \qquad (15)$$

which states that T_β can be decomposed into an average part $\langle T_\beta \rangle^\beta$ and a deviatoric part T'_β. The formula (15) is needed in the evaluation of the convection term in (4). Inherent in the derivation is also the following heat flux jump condition

$$\lambda_\beta \nabla T_\beta \cdot \mathbf{n}_{\beta\sigma}|_{\mathcal{A}} = (\lambda_\sigma \nabla T_\sigma - \Delta H \rho_\beta \mathbf{u}) \cdot \mathbf{n}_{\beta\sigma}|_{\mathcal{A}}$$

which has been used in conjunction with the assumption of a continuous temperature $T|_{\mathcal{A}} = T_\beta|_{\mathcal{A}} = T_\sigma|_{\mathcal{A}}$ at the interface $\mathcal{A}$ of the two phases. Furthermore, to close the LVA equation after application of (7), (8) and (15) to (4) and (5), a gradient hypothesis has been applied

$$\begin{aligned} \mathbf{\Lambda}_{\text{eff}} \cdot \nabla \langle T \rangle = [\varepsilon \lambda_\beta + (1-\varepsilon)\lambda_\sigma] \nabla \langle T \rangle + \\ \frac{\lambda_\beta - \lambda_\sigma}{\mathcal{V}} \int_{\mathcal{A}} T \mathbf{n}_{\beta\sigma} \, dA - \langle \rho_\beta \rangle^\beta c_{p,\beta} \langle \mathbf{u}' T'_\beta \rangle \end{aligned} \qquad (16)$$

such that the effective thermal conductivity tensor $\mathbf{\Lambda}_{\text{eff}}$ is composed of two parts

$$\mathbf{\Lambda}_{\text{eff}} = \mathbf{\Lambda}_{\text{stag}} + \mathbf{\Lambda}_{\text{disp}} = \lambda_{\text{stag}} \mathbf{I} + \mathbf{\Lambda}_{\text{disp}}$$

Here, the stagnant thermal conductivity tensor $\mathbf{\Lambda}_{\text{stag}}$, which reduces to a scalar due to isotropy, accounts for the first two terms on the right hand side of (16) and the thermal dispersion tensor $\mathbf{\Lambda}_{\text{disp}}$ accounts for the last term. To determine λ_{stag} the expression of Hadley [15], which compares nicely to experimental data for a wide range of $\kappa = \lambda_\sigma / \lambda_\beta$, is used

$$\begin{aligned} \lambda_{\text{stag}}/\lambda_\beta = (1-\alpha) \frac{\varepsilon f_0 + \kappa(1-\varepsilon f_0)}{1-\varepsilon(1-f_0)+\kappa\varepsilon(1-f_0)} + \\ \alpha \frac{2\kappa^2(1-\varepsilon)+(1+2\varepsilon)\kappa}{(2+\varepsilon)\kappa+1-\varepsilon} \end{aligned}$$

where α and f_0 are given by

$$\log \alpha = -1.084 - 6.778(\varepsilon - 0.298) \text{ and } f_0 = 0.8 + 0.1\varepsilon$$

As is the case with λ_{stag}, there are many different correlations for $\mathbf{\Lambda}_{\text{disp}}$ in the literature. In this paper the correlation proposed by Metzger *et al.* [16] is applied due to its simplicity and applicability for a wide range of Péclet numbers. Their expression for the longitudinal dispersion component is

$$(\Lambda_{\text{disp}})_{ii}/\lambda_\beta = 0.073 \text{Pe}_{d_p,i}^{1.59}, \quad i = 1, \ldots, d$$

and the Péclet number based on the particle diameter and the Darcian velocity is $\text{Pe}_{d_p,i} = (\rho c_p)_\beta |\langle u \rangle_i| d_p / \lambda_\beta$ for $i = 1, \ldots, d$. In this work the contribution from the lateral dispersion component is disregarded since it is typically an order of magnitude smaller than the longitudinal dispersion component. In the tank walls the effective thermal conductivity tensor simplifies to $\Lambda_{\text{eff}}|_{\Omega_w} = \lambda_{\text{steel}}$.

NUMERICAL METHODS

In this paper the spectral element method SEM is applied for the spatial discretization. This method is based on the solution of the weak form of the governing equations using high order Legendre polynomials of degree N, within each element, as basis functions combined with Gauss-Lobatto-Legendre (GLL) quadrature. The method typically exhibits exponential convergence rates in space such that fewer degrees of freedom are needed, to reach a given error target, compared to low order methods like the finite element method. For details, the reader might consult Ref. [17].

To advance the equations forward in time the third order backward differentiation formula BDF3 is used. However, since the equations are coupled and non-linear, extrapolations of relevant terms are needed in order to facilitate a sequential solution procedure. Furthermore, the Uzawa algorithm is applied to solve (12)-(13). The Uzawa equation is derived by performing a block Gaussian elimination of the discrete system of equations resulting from the discretization of (12)-(13), see e.g. Ref. [18]. Since the Uzawa operator is non-symmetric in this case, due to the use of cylindrical coordinates, the biconjugate gradient stabilized BICGSTAB algorithm is applied to solve it. Nested iterations are not needed here, since the discrete viscous operator is diagonal. The Uzawa algorithm is combined with the $\mathbb{P}_N$-$\mathbb{P}_{N-2}$-method to avoid any spurious pressure modes. The overall solution strategy to advance the equations from time-level t^n to t^{n+1} is then:

1. Solve the LDF equation (9) for $\langle \rho_{\text{ad}} \rangle^{n+1}$ with an extrapolated value for $\langle \rho^*_{\text{ad}} \rangle^{n+1}$ and calculate the volumetric adsorption rate $\langle \dot{\rho}_{\text{ad}} \rangle^{n+1}$.
2. Solve the Uzawa equation for pressure $(\langle p \rangle^\beta)^{n+1}$ with an extrapolated value for $\langle \rho_\beta \rangle^\beta$.
3. Calculate the velocity field $\langle \mathbf{u} \rangle^{n+1}$ from (12). This is done explicitly since the SEM mass matrix is diagonal.

4. Solve the energy equation (14) for the temperature $\langle T\rangle^{n+1}$.
5. Calculate the gas phase density $(\langle\rho_\beta\rangle^\beta)^{n+1}$ with the ideal gas law.

The energy equation is also solved with BICGSTAB as the coefficient matrix is non-symmetric due to the convection operator.

NUMERICAL SIMULATIONS AND DISCUSSION

Given the cylindrical geometry of the tank, the governing equations are written in cylindrical coordinates $\mathbf{x} = (r, z)$ and symmetry is assumed in the angular direction. The computational domain is given by $\Omega = (0, R_o) \times (0, H) \in \mathbb{R}^2$, where R_o is the outer tank radius and H is the tank height. The model has been solved using $E = 12$ spectral elements, see Fig. 5c for the partitioning of Ω into spectral elements, with $N = 7$ order polynomials for the basis functions and a time-step of size $h = 1/4$. This time-step is mainly chosen to prevent that BDF3 produces undershoots in the calculation of $\langle\rho_{\text{ad}}\rangle$. With these settings the numerical error is well below the modeling error. Parameters and property values related to the mathematical model are given in Tab. 1.

Parameter	Symbol	Value	Ref.
Activation energy	E_A	4.32 kJ/mol	[11]
Pre-exp. factor	A	$1.32 \cdot 10^{-3}$ MPa^{-1}	[11]
Gas constant	R	8314 J/(kmol·K)	-
Molecular weight	M_{H_2}	2.016 kg/kmol	-
NORIT spec. surf. area	SSA_{NOR}	1320 m^2/g	[12]
AX-21 spec. surf. area	SSA_{AX}	2800 m^2/g	[11]
Porosity	ε	0.4	[12, 19]
Micro-porosity	ε_μ	0.3	[12, 19]
Particle diameter	d_p	$2.4 \cdot 10^{-3}$ m	[19]
Viscosity	μ	$4.21 \cdot 10^{-6}$ kg/(m·s)	[20]
H_2 therm. cond.	λ_β	0.14 W/(m·K)	[20]
Carbon therm. cond.	λ_σ	20 W/(m·K)	-
Steel therm. cond.	λ_{steel}	15 W/(m·K)	[20]
Hydrogen spec. heat	$c_{p,\beta}$	14000 kJ/(kg·K)	[20]
Carbon spec. heat	$c_{p,\sigma}$	725 kJ/(kg·K)	[5]
Carbon density	$\langle\rho_\sigma\rangle$	400.0 kg/m^3	[19]
Self-diffusivity	$\mathscr{D}$	$2.5 \cdot 10^{-6}$ m^2/s	-
Heat of adsorption	$-\Delta H$	4.66 kJ/mol	[11]
Tank height	H	$723.5 \cdot 10^{-3}$ m	-
Wall thickness	d_w	$3.5 \cdot 10^{-3}$ m	-
Outer tank radius	R_o	$69.5 \cdot 10^{-3}$ m	-

Table 1: Model parameters with citations to the references from which they were obtained. The porosity ε has been deduced from Refs. [12, 19].

As mentioned in the introduction we wish to investigate the behavior of the vessel during charging. The charging time t_{fill} is defined as the time needed to reach a certain fraction κ

$$\kappa = m(p, \langle T\rangle)/m_{\max}(p_{\text{fill}}, T_{\text{N}_2})$$

of the maximum storage capacity at a given filling pressure. The stored mass m is calculated by applying GLL quadrature to the integral

$$m(p, T) = 2\pi \int_0^H \int_0^{R_o} \rho_{\text{tot}}(p, \langle T\rangle) r \, dr dz$$

Boundary- and initial conditions. Denoting the boundary of Ω by Γ it is divided into the inlet $\Gamma_1 = \{(r, z) \in \Gamma, 0 \le r \le R_{\text{inlet}}, z = H\}$, the centerline $\Gamma_2 = \{(r, z) \in \Gamma, r = 0\}$ and the outer surface of the tank walls in contact with the liquid nitrogen $\Gamma_3 = \Gamma - \Gamma_1 \cup \Gamma_2$. The boundary conditions for the momentum- and continuity equations (12)-(13) are

$$\langle p\rangle^\beta|_{\Gamma_1} = -p_{\text{fill}} \tag{17}$$

$$\mathbf{u} \cdot \mathbf{n}|_{\Gamma_2} = 0 \tag{18}$$

where $\mathbf{u} = (u, v)^T$. Here, (17) is imposed weakly and (18) states that no mass can cross a symmetry line. In addition, the inner tank walls are impermeable such that $\mathbf{u} \cdot \mathbf{n} = 0$ at the interface between the porous bed and the inner tank walls. For the energy equation (14) the boundary conditions are given as

$$(\mathbf{\Lambda}_{\text{eff}} \cdot \nabla\langle T\rangle) \cdot \mathbf{n}|_{\Gamma_1} = (\rho c_p)_\beta \langle\mathbf{u}\rangle(\langle T\rangle - T_{\text{fill}}) \cdot \mathbf{n}|_{\Gamma_1}$$
$$(\mathbf{\Lambda}_{\text{eff}} \cdot \nabla\langle T\rangle) \cdot \mathbf{n}|_{\Gamma_2} = 0$$
$$\langle T\rangle|_{\Gamma_3} = T_{\text{N}_2}$$

where $T_{\text{N}_2} = 77$ K is the temperature of the liquid nitrogen bath and $T_{\text{fill}} = 273$ K is the temperature of the incoming hydrogen. The initial conditions ($t = 0$) are set to

$$\langle\mathbf{u}\rangle_0 = 0, \ \langle T\rangle_0 = 77 \text{ K}, \ \langle p\rangle_0^\beta = 1 \text{ bar}$$

and $\langle\rho_{\text{ad}}\rangle_0$ and $\langle\rho_\beta\rangle_0^\beta$ are initialized thereafter. Being an ODE, (9) only needs an initial condition.

Interpretation of results. A series of simulations have been conducted with filling pressures ranging from 5 to 40 bars and $\kappa \in \{0.85, 0.90, 0.95\}$. These runs are summarized in Fig. 4 which shows t_{fill} as function of p_{fill} for different values of κ. It can be seen that t_{fill} decreases with p_{fill}.

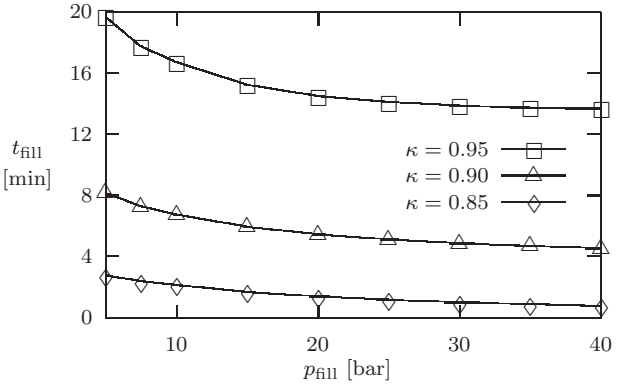

Figure 4: Filling time t_{fill} as a function of filling pressure p_{fill} to reach a given fraction κ of the maximum storage capacity.

This seemingly non-intuitive behavior can be explained

by the fact that the ratio of gaseous- and adsorbed hydrogen $\langle\rho_\beta\rangle^\beta/\langle\rho_{\rm ad}\rangle$ increases with pressure. The density of gaseous hydrogen $\langle\rho_\beta\rangle^\beta$ approaches its maximum value faster than $\langle\rho_{\rm ad}\rangle$ when the tank is cooled which implies that the bed temperature at $t_{\rm fill}$ can be higher at elevated pressures. Consequently, part of the problem of poor heat transfer rates, when the tank approaches thermal equilibrium with the nitrogen bath, is avoided. In general, at high $p_{\rm fill}$ more energy is introduced to the system by inflowing hydrogen. The increased heat input does not seem to restrict the charging time considerably. It can be argued that the introduced heat is efficiently dissipated to the nitrogen in the dewar by the sharp radial temperature gradients close to the entrance.

Temperature fields at different time levels for one particular realization with $p_{\rm fill} = 40$ bar and $\kappa = 0.95$ are shown in Fig. 5a-b. These figures show the heating of the tank at the inlet due to the incoming hydrogen gas and the heating downstream due to adsorption. The temperature decreases rather rapidly in the axial direction since the incoming mass is cooled from the side by the liquid nitrogen bath and by the thermal mass already present in the tank. The axial decrease of temperature is also due to the small convecting velocities. In fact, apart from a limited time period immediately after start up, thermal convection is negligible. Hence, the filling process is reduced to a thermal conduction problem.

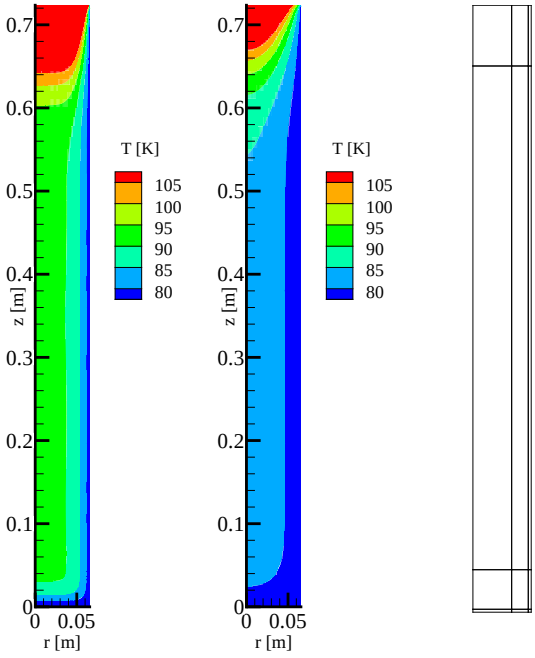

Figure 5: The temperature field at (a) $t = 0.10 \cdot t_{\rm fill}$ and (b) $t = 0.90 \cdot t_{\rm fill}$ for the case with $p_{\rm fill} = 40$ bar and $\kappa = 0.95$. (c) The spectral element partitioning of Ω.

Fig. 5 also serves as a reminder of the shortcomings of the model. The aforementioned assumption of semi-incompressibility, i.e. $\partial\rho/\partial t = 0$, reduces the pressure to a non-physical variable. As a consequence the tank pressure increases too rapidly and the volumetric adsorption rate $\langle\dot\rho_{\rm ad}\rangle$ becomes close to uniform in space. This is in contrast to the actual adsorption process which one would believe to have a high rate close to the inlet and then gradually increase downstream as the pressure builds up. Despite the limitation the model still offers valuable information as it estimates lower bounds for charging times.

FINAL REMARKS

We have presented a mathematical model and created a numerical test bed for the analysis of transient behavior of transport processes in a hydrogen adsorption storage tank. It was deduced from the numerical experiments that the poor effective thermal conductivity of the porous bed limits rapid filling. Therefore, it can be argued that for real life storage systems based on adsorption an efficient charging strategy is needed that incorporates the issue of thermal management. Finally, it is mentioned that the work presented herein will be the backbone of forthcoming numerical studies including heat and mass transfer enhancement, improvement of mathematical model to allow for compressibility, parameter sensitivity analysis and validation based on anticipated experimental data.

REFERENCES

[1] F Askri et al. *Int. J. Hydrogen Energy*, 29(2):195–208, 2004.
[2] A Dogan et al. *Applied Mathematics and Computation*, 150 (1):169–180, 2004.
[3] A Jemni and B Nasrallah. *Int. J. Hydrogen Energy*, 20(1): 43–52, 1995.
[4] M Lamari et al. *Environmental and Energy Engineering*, 46 (3):632–646, 2000.
[5] A Delahaye et al. *Energy and Environmental Engineering*, 48 (9):2061–2073, 2002.
[6] S Whitaker. Theory and Applications of Transport in Porous Media. Kluwer Academic Press, 1999.
[7] S Sircar and J R Hufton. *Adsorption*, 6(2):137–147, 2000.
[8] J H Hills. *Chemical Engineering Science*, 41(11):2779–2785, 1986.
[9] G H Neale and W K Nader. *AIChE J.*, 19(1):112–119, 1973.
[10] B Panella et al. *Carbon*, 43(10):2209–2214, 2005.
[11] P Bénard and R Chahine. *Langmuir*, 17(6):1950–1955, 2001.
[12] N Texier-Mandoki et al. *Carbon*, 42(12-13):2744–2747, 2004.
[13] P Bénard and R Chahine. *Int. J. Hydrogen Energy*, 26(13): 849–855, 2001.
[14] S Whitaker. *Transport in Porous Media*, 25(1):27–61, 1996.
[15] G R Hadley. *Int. J. Heat and Mass Transfer*, 29(6):909–920, 1986.
[16] T Metzger et al. *Int. J. Heat and Mass Transfer*, 47(14-16): 3341–3353, 2004.
[17] M O Deville et al. Cambridge Monographs on Applied and Computational Mathematics. Cambridge University Press, 2002.
[18] Y Maday, D Meiron, A T Patera, and E M Rønquist. *SIAM J. Sci. Comput.*, 14:310–337, 1993.
[19] Norit Digital Library. Norit R0.8 datasheet, 2005.
[20] A F Mills. Series in Heat Transfer. Richard D Irwin, Inc., 1995.